RSC Advances

PAPER

View Article Online
View Journal | View Issue

Cite this: *RSC Adv.*, 2017, **7**, 40046

Upconversion luminescence and temperature-sensing properties of Ho^{3+}/Yb^{3+}-codoped $ZnWO_4$ phosphors based on fluorescence intensity ratios

Xiaona Chai, Jun Li, Xusheng Wang,* Yanxia Li and Xi Yao

Received 24th May 2017
Accepted 24th July 2017

DOI: 10.1039/c7ra05846b

rsc.li/rsc-advances

Ho^{3+}/Yb^{3+}-codoped $ZnWO_4$ phosphors were synthesized using a solid state reaction method and their structures, upconversion (UC) luminescence, and temperature-sensing properties were investigated. The obtained $ZnWO_4$:0.01Ho^{3+}/xYb^{3+} phosphors crystallized in the monoclinic phase with space group *P*2/*c*. Under 980 nm excitation, bright green [($^5F_4$, $^5S_2$) → $^5I_8$], weak red ($^5F_5$ → $^5I_8$), and near-infrared emissions [($^5F_4$, $^5S_2$) → $^5I_7$] were observed. The optimal Ho^{3+} and Yb^{3+} doping concentrations in $ZnWO_4$ were 0.01 and 0.15, respectively. The near-infrared-green (I_{757}/I_{540}) and red-green ($I_{641,665}/I_{540,549}$) fluorescence intensity ratios (FIRs) were studied as a function of temperature at 83–503 K. The sensitivity of the $ZnWO_4$:0.01Ho^{3+}/0.15Yb^{3+} phosphors was also discussed and their potential application as thermal sensors in luminescence thermometry was analyzed using a four-level system and the intensity ratio of the red and green emissions. $ZnWO_4$:0.01Ho^{3+}/0.15Yb^{3+} phosphors could potentially be applied as optical temperature-sensing materials.

1. Introduction

Noncontact temperature measurement has recently attracted much interest for its ability to measure high temperatures and characterize moving surfaces, even in the presence of strong electromagnetic fields, without interference.[1] Rare earth elements exhibit narrow emission and absorption lines, and relatively long emission lifetimes. Therefore, rare-earth-doped materials have been applied in temperature sensors using luminescent thermometry techniques. Among rare earths, Ho^{3+} has been verified as a promising candidate in addition to Er^{3+}. The thermally coupled levels of Ho^{3+} ions, namely $^5F_4$ and $^5S_2$, $^5F_3$ and $^3K_8$, and $^5F_{2,3}/^3K_8$ and $^5G_6/^5F_1$, have been investigated in temperature sensing.[2–9] Yb^{3+} ions coupled to Ho^{3+} are usually used as sensitizers due to their larger absorption cross-section in the near-infrared region and the efficient energy transfer from Yb^{3+} to Ho^{3+}.

Compared with conventional contact temperature measurement methods, the noncontact fluorescence intensity ratio (FIR) technique is considered a promising approach to temperature sensing because it can reduce the dependence on measurement conditions and improve accuracy.[10–12] Therefore, noncontact optical sensors based on FIR thermometry are particularly suitable for monitoring temperature under harsh conditions, such as electrical, magnetic, and electromagnetic fields, and flammable situations. In general, the FIR method can be used for temperature measurement if the FIR varies monotonically with temperature in rare-earth-doped materials.

Tungstates with monoclinic structures, which possess high chemical and physical stability and superior intrinsic luminescent properties, are considered good luminescent hosts. Among them, $ZnWO_4$ has shown good properties as a scintillator crystal,[13] while phosphors, such as $ZnWO_4$ materials doped with rare earth ions (Er, Dy, Ho, Eu), showed excellent fluorescence properties.[14–20] Furthermore, $ZnWO_4$ has other advantages that benefit upconversion (UC), such as a low phonon threshold energy (199.5 cm^{-1}).[21,22] Therefore, $ZnWO_4$ is a potential luminescent material. However, the upconversion luminescence and temperature-sensing capabilities of Ho^{3+} ion-doped $ZnWO_4$ systems have not been studied.

In this context, $ZnWO_4$:0.01Ho^{3+}/xYb^{3+} phosphors were prepared using a typical solid-state reaction method and their room-temperature UC emission properties and energy transfer (ET) mechanism were analyzed. The near-infrared-green FIR (I_{757}/I_{540}) and red-green FIR ($I_{641,665}/I_{540,549}$) were studied as a function of temperature from 83 K to 503 K. For the near-infrared-green FIR (I_{757}/I_{540}), the four-level FIR system was used to analyze the optical temperature sensing of $ZnWO_4$:0.01Ho^{3+}/xYb^{3+} phosphors, while for the red-green FIR ($I_{665,641}/I_{540,549}$), we explored using the intensity ratio of red and green emissions generated from linked electronic states, which provided a new route for temperature measurement.

Key Laboratory of Advanced Civil Engineering Materials of the Ministry of Education, Functional Materials Research Laboratory, School of Materials Science and Engineering, Tongji University, 4800 Cao'an Road, Shanghai 201804, China. E-mail: xs-wang@tongji.edu.cn

2. Experimental

Ho^{3+}/Yb^{3+} codoped $ZnWO_4$ phosphors ($ZnWO_4$:0.01Ho^{3+}/xYb^{3+}) were synthesized using a conventional solid state reaction method. The Ho^{3+} ion concentration was fixed at 1 mol%, while the Yb^{3+} concentration was varied (x = 0.01, 0.02, 0.04, 0.06, 0.08, 0.10, 0.15, 0.20). High-purity ZnO, WO_3, Er_2O_3, and Ho_2O_3 powders were weighed and ground thoroughly for 2 h using an agate mortar. The mixed powders were then calcined at 750 °C for 5 h. The calcined powders were reground for 1 h, an mixed thoroughly with PVA binder solution (10 wt%), and then pressed into pellets (diameter, 10 mm; thickness, approx. 2 mm). Finally, the samples were sintered at 1100 °C for 4 h in an alumina crucible in air. To ensure the luminescence measurements were accurate, the sintered pellets were ground to the same thickness.

The basic crystal structures of $ZnWO_4$:0.01Ho^{3+}/xYb^{3+} phosphors were examined using X-ray diffraction (XRD; D/MAX 2550, Rigaku, Japan) with Cu Kα radiation at room temperature. Sample XRD profiles were collected in the 2θ range of 10–90° with a scanning speed of 5° min^{-1}. UC photoluminescence emission spectra were measured using a fluorescence spectrofluorometer (F-7000, Hitachi, Japan) under excitation by a 980 nm diode laser. The phosphor temperatures were controlled in the range 83–583 K using a TP94 temperature controller (Linkam Scientific Instruments Ltd, Surrey, UK).

3. Results and discussion

3.1 XRD analysis

The XRD patterns of the $ZnWO_4$:0.01Ho^{3+}/xYb^{3+} samples are shown in Fig. 1(a). The main peaks were easily matched and indexed based on the standard diffraction data for $ZnWO_4$ with a monoclinic structure (PDF#89-0447). This observation indicated that, as desired, the Ho^{3+}/Yb^{3+} ions may have diffused into the A site of the $ZnWO_4$ host structure. Codoping with 1 mol% Ho^{3+} and 1 mol% Yb^{3+} did not change the crystal structure of the material. With increasing Yb^{3+} concentration ($x \leq 0.08$), the samples still showed a single-phase monoclinic structure. However, a second phase of Yb_2WO_6 was observed when the Yb^{3+} concentration exceeded 8 mol%. These results indicated that the solid solubility limit of Yb^{3+} ions in $ZnWO_4$:0.01Ho^{3+} materials was 8 mol%. Furthermore, sample diffraction peaks near the (111) peaks gradually shifted to lower angles with increasing Yb^{3+} doping concentration (Fig. 1(b)). These shifts were clearly attributed to differences among the ionic radii of Ho^{3+}/Yb^{3+} (CN = 6, 0.901 Å and 0.868 Å),[23] Zn^{2+} (CN = 6, 0.74 Å),[24] and W^{6+} (CN = 6, 0.60 Å),[24] resulting in an increase in unit cell volume and diffraction peak shift.

3.2 Upconversion luminescence properties

Under excitation with a 980 nm near-infrared laser, all Ho^{3+}/Yb^{3+}-codoped $ZnWO_4$ phosphors exhibited strong green UC emissions at room temperature (Fig. 2). The emission bands at around 520–580 nm, 630–680 nm, and 735–775 nm were assigned to ($^5F_4$, $^5S_2$) → $^5I_8$, $^5F_5$ → $^5I_8$, and ($^5F_4$, $^5S_2$) → $^5I_7$ transitions, respectively. All emission bands were in good agreement with previous reports on other Ho^{3+}-doped materials.[7,25–27] Among the three emission bands, the green emission originating from the ($^5F_4$, $^5S_2$) → $^5I_8$ transition was the strongest, resulting in a strong green emission observed in Ho^{3+}/Yb^{3+}-codoped $ZnWO_4$ phosphors. As shown in Fig. 2, when the concentration of Ho^{3+} was fixed at 1 mol%, the UC emission intensity increased gradually with increasing Yb^{3+} concentration, reaching a maximum value when the Yb^{3+} concentration (x = 0.15) was 15 times that of Ho^{3+}. The emission intensity decreased if the Yb^{3+} concentration exceeded this critical value (x = 0.15). Yb^{3+} ion is known as a highly efficient sensitizer of Ho^{3+} ions due to its larger near-infrared absorption cross-section. The Yb^{3+} to Ho^{3+} energy transfer (ET) process was enhanced by increasing the Yb^{3+} concentration from 0.01 to 0.15, yielding a higher UC emission intensity. However, the distance between neighboring Yb^{3+} ions became shorter with increasing Yb^{3+} concentration. This resulted in stronger interactions between neighboring Yb^{3+} ions, which led to concentration-dependent quenching.

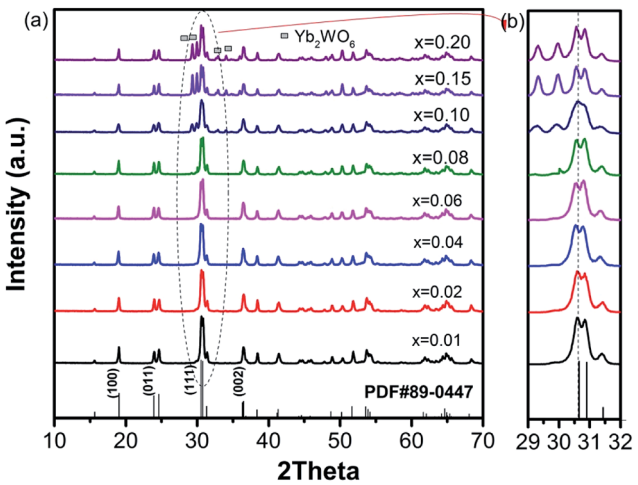

Fig. 1 XRD patterns of $ZnWO_4$:0.01Ho^{3+}/xYb^{3+} samples in the 2θ range of (a) 10–70° and (b) 29–32°.

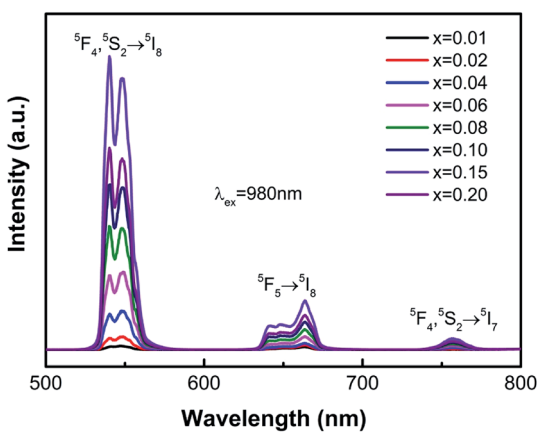

Fig. 2 Upconversion emission (λ_{ex} = 980 nm) spectra of $ZnWO_4$:0.01Ho^{3+}/xYb^{3+} phosphors at room temperature.

Fig. 3 shows the schematic energy level diagram of Ho^{3+} and Yb^{3+} ions. Under 980 nm laser excitation, Yb^{3+} ions absorbed an infrared photon (980 nm), transited from ground state $^2F_{7/2}$ (GSA) to excited state $^2F_{5/2}$, and then transferred the energy to Ho^{3+} ions, populating the $^5I_6$ state of Ho^{3+} ions. Subsequently, Ho^{3+} ions excited to $^5I_6$ might be further excited to the ($^5F_4$, $^5S_2$) coupling state by ET ($^5I_6 + {}^2F_{5/2} \rightarrow {}^5F_4$, $^5S_2 + {}^2F_{7/2}$) or excited state absorption (ESA; $^5I_6 + h\nu \rightarrow {}^5F_4$, $^5S_2$). The transition from ($^5F_4$, $^5S_2$) to $^5I_8$ states produced a strong green emission. However, the red emission was attributed to the transition from $^5F_5$ to $^5I_8$. Three processes might contribute to populating the $^5F_5$ state. The first involved the intermediary level $^5I_6$ of Ho^{3+} relaxing to $^5I_7$ by nonradiative transition and then populating the $^5F_5$ state by absorbing another photon *via* ESA. The second involved a nonradiative relaxation process from the $^5F_4$, $^5S_2$ state to the $^5F_5$ state. The last process involved cross-relaxation between two Ho^{3+} ions ($^5F_4$, $^5S_2 + {}^5I_7 \rightarrow {}^5F_5 + {}^5I_6$). At lower Ho^{3+} ion concentrations, the third process had a low probability in the UC process. Therefore, the first two processes were dominant in populating the $^5F_5$ level. The near-infrared UC luminescence emission was due to $^5F_4$, $^5S_2 \rightarrow {}^5I_7$ transitions.

To better understand the UC emission process of Ho^{3+}/Yb^{3+}-codoped $ZnWO_4$ phosphors, the dependence of the UC emission spectra of $ZnWO_4$:0.01Ho^{3+}/0.15Yb^{3+} ceramic on pump power was examined, as shown in Fig. 4(a). The peak values of all peaks increased gradually with increasing power in the range 80–240 mW. For the UC process, the emission band intensity (I) was proportional to the exponent (n) of pump power (P), with their relationship described by the formula, $I \propto P^n$,[28,29] where n denotes the number of photons involved in the pumping mechanism, which can be determined from the slope of the straight line obtained by plotting ln(I) *vs.* ln(P). Fig. 4(b) shows experimental data and fitting curves for $ZnWO_4$:0.01Ho^{3+}/0.15Yb^{3+} ceramic. The plots of ln(I) *vs.* ln(P) showed n values of 1.96, 1.83, and 2.11 for green, red, and near-infrared emissions, respectively. The slope values were near 2, which indicated that a two-photon UC mechanism was involved in all three emission processes. Fig. 4(c) shows the CIE chromaticity diagram, which is used to study color perception in terms of mathematically defined color spaces. The relevant boxed section in Fig. 4(c) has been enlarged. A yellowish-green color perception with coordinates of (0.32, 0.64) was obtained using a low laser power (20 mW) emission, and the color coordinates moved toward the pure green region with increasing excitation power. However, the color coordinates were almost unchanged when increasing the excitation power continuously from 40 mW (0.31, 0.67) to 240 mW (0.31, 0.68), indicating that the sample emission color was not meaningfully affected by the pump power.

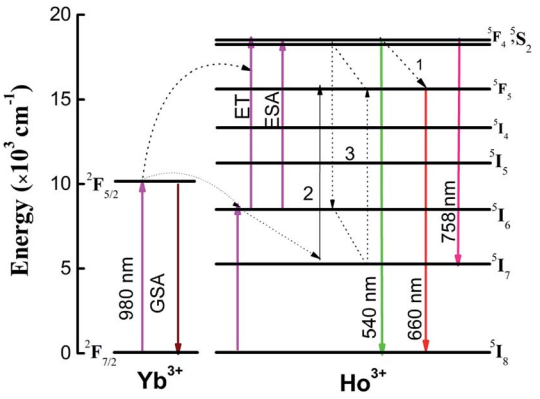

Fig. 3 Energy level schematic diagram of Ho^{3+} and Yb^{3+} ions, and the proposed upconversion luminescence mechanism in $ZnWO_4$.

3.3 Optical temperature-sensing properties

Optical temperature sensing is among the most important applications of UC emission materials. Herein, the optical temperature-sensing properties of $ZnWO_4$:0.01Ho^{3+}/0.15Yb^{3+} were analyzed using the FIR technique. For this purpose, the UC emission spectra of the $ZnWO_4$:0.01Ho^{3+}/0.15Yb^{3+} ceramic in the temperature range 83–503 K were investigated. Fig. 5(a) shows the UC emission spectra for $ZnWO_4$:0.01Ho^{3+}/0.15Yb^{3+} ceramic at 123, 203, 363, 443, and 523 K, with the spectra normalized to the most intense emission peak at 540 nm. No significant shift was observed for all UC emission bands. With increasing temperature, the green UC emissions decreased due to thermal quenching effect (see Fig. 5(a) inset). Based on previous reports, thermalization between the $^5S_2$ and $^5F_4$ levels was analyzed using a four-level FIR system. This system consists of four levels, namely $^5I_8$ (level 1), $^5I_7$ (level 2), $^5S_2$ (level 3), and $^5F_4$ (level 4), and was introduced by Haro-González *et al.*,[30] as shown in Fig. 5(b). The energy gap between the $^5F_4$ and $^5S_2$ levels (ΔE) is about 120 cm^{-1}.[30] Therefore, populating the $^5F_4$ level from the $^5S_2$ level can be achieved by thermal excitation. Accordingly, the ratio of the bands at 540 nm and 757 nm (FIR) followed a Boltzmann-type distribution. The FIR can be described using eqn (1):[31]

$$\mathrm{FIR} = \frac{I_1 + I_{1'}}{I_2 + I_{2'}} = \frac{I_{754}}{I_{540}} = \frac{\omega_{42} g_4 h\nu_{41} \exp(-\Delta E/kT) + \omega_{32} g_3 h\nu_{31}}{\omega_{41} g_4 h\nu_{42} \exp(-\Delta E/kT) + \omega_{31} g_3 h\nu_{32}} = \frac{C_1 + C_2 \exp(-\Delta E/kT)}{C_3 + C_4 \exp(-\Delta E/kT)} \quad (1)$$

where I_{754} and I_{540} are the intensities of upconversion emissions from the upper ($^5F_4$) and lower ($^5S_2$) thermally coupled levels, g_4 and g_3 are the degeneracy ($2J + 1$) of the $^5F_4$ and $^5S_2$ levels, ω_{41}/ω_{42} and ω_{31}/ω_{32} are the spontaneous emission rates of the $^5F_4/^5S_2$ levels to the $^5I_8$ level and level 2, respectively, and $h\nu$ is the transition energy. ΔE is the energy gap between the $^5F_4$ and $^5S_2$ levels, k is the Boltzmann constant, and T is the absolute temperature.

Fig. 5(c) showed the dependence of FIR on absolute temperature for the $ZnWO_4$:0.01Ho^{3+}/0.15Yb^{3+} phosphor. The FIR value decreased gradually with increasing temperature, reaching the minimum value at the maximum measured temperature. The solid line represents FIR obtained by fitting the experiment data. The curves matched well with the experimental data for $ZnWO_4$ crystals. From Fig. 5(b), the fitted values of C_1, C_2, C_3, C_4, and energy gap ΔE were −0.10, 0.66, 2.08, 3.88, and 168.3 cm^{-1}, respectively.

For optical thermometry applications, it is important to know the sensitivity (S). Similar to the three-level system, S can be defined using eqn (2):

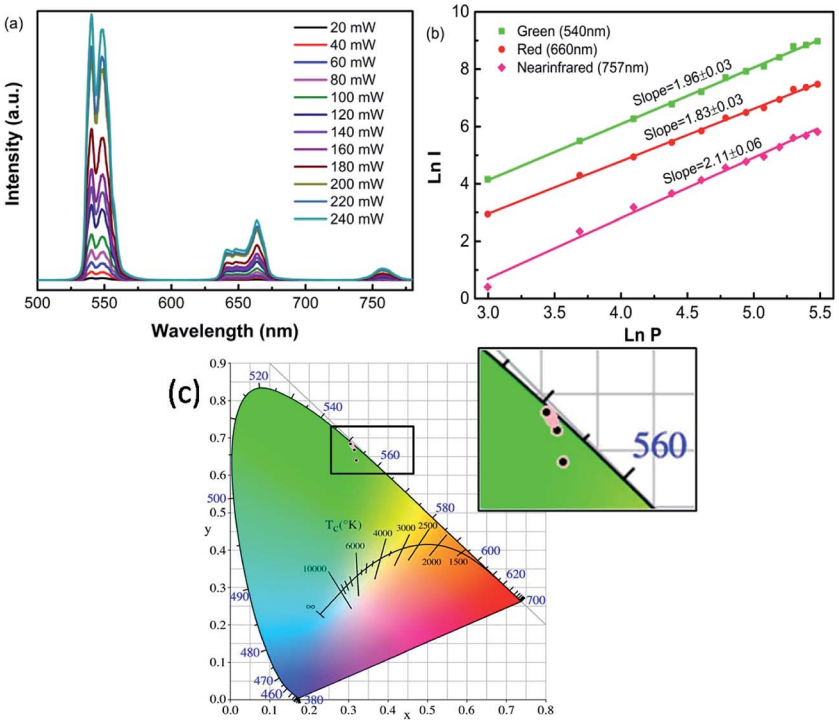

Fig. 4 (a) UC spectra of $ZnWO_4$:0.01Ho^{3+}/0.15Yb^{3+} as a function of pump power at room temperature. (b) Dependence of green, red, and infrared UC emission intensities on pump power. (c) CIE chromaticity diagram of $ZnWO_4$:0.01Ho^{3+}/0.15Yb^{3+} at different pump powers.

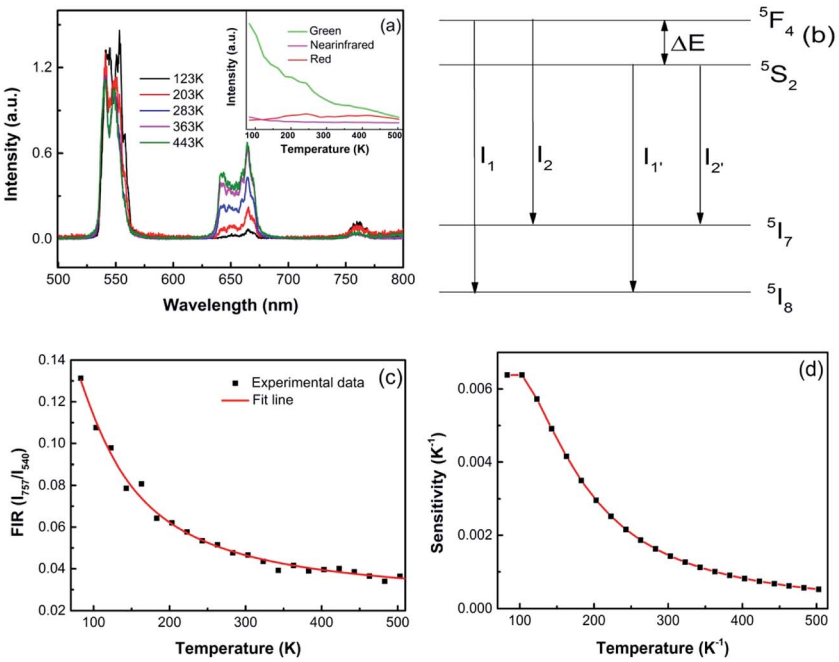

Fig. 5 (a) UC emission spectra of $ZnWO_4$:0.01Ho^{3+}/0.15Yb^{3+} at different temperatures; inset, plot of upconversion intensity *vs.* temperature. (b) A simplified four-level system diagram. (c) FIR of I_{757}/I_{540} at 83–503 K. (d) Sensitivity graph for the I_{757}/I_{540} ratio.

$$S = \frac{\mathrm{dFIR}}{\mathrm{d}T} = \frac{(C_2 \times C_3 - C_1 \times C_4)\dfrac{\Delta E}{kT^2}\exp\left(-\dfrac{\Delta E}{kT}\right)}{\left[C_3 + C_4 \exp\left(-\dfrac{\Delta E}{kT}\right)\right]^2} \quad (2)$$

The calculated sensitivity as a function of temperature is shown in Fig. 5(d). The sensitivities decreased continuously with increasing temperature within the experimental temperature range. The maximum S value of about 0.0064 K^{-1} was obtained at 83 K. Therefore, Ho^{3+}/Yb^{3+}-codoped $ZnWO_4$ crystals

Table 1 Optical temperature-sensing properties of Ho-doped materials using the FIR technique

Materials	Temperature (K)	Excitation wavelength (nm)	Transitions	S_{max} (K^{-1})	References
Ho:In–Zn–Sr–Ba glass	20–300	473	$^5F_4/^5S_2 \rightarrow {}^5I_8, {}^5I_7$	0.0036 (59 K)	30
Ho, Yb:Y_2O_3	10–300	978	$^5F_4/^5S_2 \rightarrow {}^5I_8, {}^5I_7$	0.097(536/772) (85 K) 0.065(536/764) (84K) 0.046(536/758) (90K)	4
Ho/Yb:BCT	93–300	980	$^5F_4/^5S_2 \rightarrow {}^5I_8, {}^5I_7$	0.0053 (93 K)	31
Ho, Yb:$ZnWO_4$	83–503	980	$^5F_4/^5S_2 \rightarrow {}^5I_8, {}^5I_7$	0.0064 (83 K)	This work
Ho:TeO_2 glass	265–440	890	$^5F_4, {}^5S_2 \rightarrow {}^5I_8$	0.0098 (130 K)	2
Ho:$LiTeO_2$ glass	265–383	890	$^5F_4, {}^5S_2 \rightarrow {}^5I_8$	0.0063 (265 K)	3
Ho/Yb:PbF_2	303–643	980	$^5F_{2,3}/^3K_8, {}^5G_6/^5F_1$	0.007 (643 K)	7
Ho/Yb:$CaWO_4$	303–923	980	$^5F_{2,3}/^3K_8, {}^5G_6/^5F_1$	0.005 (923 K)	8
Ho/Yb:$NaLuF_4$	390–780	980	$^5F_{2,3}/^3K_8, {}^5G_6/^5F_1$	0.0083 (500 K)	9
Ho/Yb/Zn:Y_2O_3	299–673	980	$^5F_3, {}^3K_8 \rightarrow {}^5I_8$	0.003 (673 K)	5
Ho/Yb/Mg:$CaMoO_4$	303–543	980	$^5F_3, {}^3K_8 \rightarrow {}^5I_8$	0.0066 (353 K)	6

were better suited to low-temperature optical sensors. For comparison, the optical temperature-sensing performances of Ho^{3+}-doped materials based on the FIR technique are listed in Table 1. The sensitivity of the materials (In–Zn–Sr–Ba glass, Y_2O_3, BCT and $ZnWO_4$) was analyzed using the four-level system ($^5F_4/^5S_2 \rightarrow {}^5I_8, {}^5I_7$) in entries at the top of Table 1, while other results were based on the three-level system. Compared to other materials based on the three-level system, the maximum S value based on the four-level system was obtained at a relatively low temperature. These results showed the Ho^{3+}-doped materials were better suited to low temperature applications using this method.

The versatility of this material offered different strategies for temperature measurement using upconversion emission spectra. Fig. 5(a) shows a clear increase in red emission intensity with increasing temperature. However, the $^5F_4/^5S_2$ level (attributed to green emission) and $^5F_5$ level (attributed to red emission) were located far apart, with electronic populations that did not follow the Boltzmann-type distribution. Therefore, the FIR technique (three-level system or four-level system) is invalid. Fortunately, analysis of the schematic energy level diagram (Fig. 3) showed that the population of the $^5F_5$ level mainly occurred through three pathways, among which the nonradiative relaxation process from the $^5F_4/^5S_2$ level to $^5F_5$ level was the most effective at low Ho^{3+} doping concentrations. The process was temperature dependent, as demonstrated by the faster increase in relative intensity of the red emission with increasing temperature (Fig. 5(a)).

Based on this analysis, we considered all of these levels to be electronically coupled, and that the temperature could be measured using the ratio of red and green light.[32–34] This electronic coupling of Ho^{3+} is expressed in the plot of I_{red}/I_{green} thermal evolution depicted in Fig. 6. Four lines were present, based on the different peaks of $^5F_4/^5S_2 \rightarrow {}^5I_8$ (540 nm, 549 nm) and $^5F_5 \rightarrow {}^5I_8$ (641 nm, 665 nm) transitions. Solid lines, obtained by fitting the experimental data, were linear. The R^2 (coefficient of determination for linear fitting) value was close to 1, which indicated that the linear fitting of experiment data was reasonable. The sensitivity, determined from the slope of the fitting curve, was 0.00153, 0.00158, 0.00109, and 0.00113 K^{-1} for

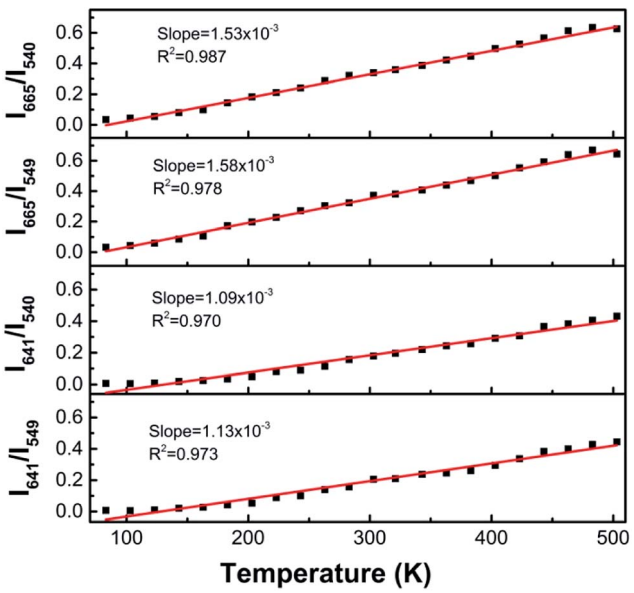

Fig. 6 Ratio of red and green emission bands as functions of temperature for $ZnWO_4$:0.01Ho^{3+}/0.15Yb^{3+}.

$^5F_4/^5S_2 \rightarrow {}^5I_8$ (540 nm, 549 nm) and $^5F_5 \rightarrow {}^5I_8$ (641 nm, 665 nm) transitions, respectively. Our research group has also studied the optical temperature sensing of Ho^{3+}/Yb^{3+}-codoped $SrBi_4Ti_4O_{15}$ (ref. 33) and $NaBi_4Ti_4O_{15}$ (ref. 34) using the intensity ratio of red and green emissions, resulting in sensitivities of 0.000493 and 0.0007 K^{-1}, respectively. In comparison, Ho^{3+}/Yb^{3+}-codoped $ZnWO_4$ showed higher sensitivities, implying that this is a versatile material for multiple thermal-sensing applications.

4. Conclusion

Ho^{3+}/Yb^{3+}-codoped $ZnWO_4$ phosphors were prepared using a high-temperature solid state method. The $ZnWO_4$:0.01Ho^{3+}/$x$$Yb^{3+}$ samples were found to crystallize in the polar monoclinic phase with space group $P2/c$ by XRD analysis. The upconversion emissions were investigated under 980 nm excitation, with the

optimal doping concentrations of Ho^{3+} and Yb^{3+} in the $ZnWO_4$ host determined to be 1 mol% and 15 mol%, respectively. A possible upconversion emission mechanism was proposed, taking into consideration the dependence of emission intensities on the pumping power, and that the green and red emissions were both related to two-photon absorption processes. Furthermore, the near-infrared-green FIR (I_{757}/I_{540}) and red-green FIR ($I_{641,\ 665}/I_{540,549}$) were studied as a function of temperature from 83 K to 503 K. The optical temperature-sensing properties were discussed based on a four-level FIR system and the ratio of red and green band intensities. The FIR (four-level system) method results showed that the highest sensitivity occurred at low temperature. However, the ratio of the red and green peak intensities showed a linear dependence on temperature. Sensitivity was constant over the thermal range tested, which allowed more precise measurements at high temperatures.

Acknowledgements

This work was supported by the National Science Foundation of China (Grant no. 51572195).

References

1 K. T. V. Grattan and Z. Y. Zhang, *Fiber Optic Fluorescence Thermometry*, Chapman and Hall, London, 1995.

2 A. K. Singh, Ho^{3+}:TeO_2 glass, a probe for temperature measurements, *Sens. Actuators, BSens. Actuators, B*, 2007, **136**(1), 173–177.

3 A. K. Singh and S. B. Rai, Upconversion and optical thermometry in Ho^{3+}:TeO_2 glass, effect of addition of PbO_2 and $BaCO_3$, *Appl. Phys. B: Photophys. Laser Chem.Appl. Phys. B*, 2007, **86**(4), 661–666.

4 V. Lojpur, M. Nikolic, L. Mancic, *et al.*, Y_2O_3: Yb,Tm and Y_2O_3:Yb,Ho powders for low-temperature thermometry based on up-conversion fluorescence, *Ceram. Int.Ceram. Int.*, 2013, **39**, 1129–1134.

5 A. Pandey and V. K. Ray, Improved Luminescence and Temperature Sensing Performance of Ho^{3+},Yb^{3+},Zn^{2+}:Y_2O_3 Phosphor, *Dalton Trans.Dalton Trans.*, 2013, **42**, 11005–11011.

6 R. Dey, A. Kumari, A.K Soni, *et al.*, $CaMoO_4$:Ho^{3+}–Yb^{3+}–Mg^{2+} upconverting phosphor for application in lighting devices and optical temperature sensing, *Sens. Actuators, BSens. Actuators, B*, 2015, **210**, 581–588.

7 W. Xu, X. Y. Gao, L. J. Zhang, Z. G. Zhang and W. W. Cao, Short-wavelength upconversion emissions in Ho^{3+}/Yb^{3+} codoped glass ceramic and the optical thermometry behavior, *Opt. ExpressOpt. Express*, 2012, **20**, 18127–18137.

8 W. Xu, H. Zhao, Y. X. Li, L. J. Zheng, Z. G. Zhang and W. W. Cao, Optical temperature sensing through the upconversion luminescence from Ho^{3+}/Yb^{3+} codoped $CaWO_4$, *Sens. Actuators, BSens. Actuators, B*, 2013, **188**, 1096–1100.

9 S. S. Zhou, S. Jiang and X. T. Wei, Optical thermometry based on upconversion luminescence in Yb^{3+}/Ho^{3+} co-doped $NaLuF_4$, *J. Alloys Compd.J. Alloy. Compd*, 2014, **588**, 654–657.

10 S. A. Wade, S. F. Collins and G. W. Baxter, Fluorescence intensity ratio technique for optical fiber point temperature sensing, *J. Appl. Phys.*, 2003, **94**, 4743–4756.

11 L. H. Fischer, G. S. Harms and O. S. Wolfbeis, Upconverting nanoparticles for nanoscale thermometry, *Angew. Chem., Int. Ed.*, 2011, **50**, 4546–4551.

12 A. Sedlmeiter, D. E. Achatz, L. H. Fischer, H. H. Gorris and O. S. Wolfbeis, Photon upconverting nanoparticles for luminescent sensing of temperature, *Nanoscale*, 2012, **4**, 7090–7096.

13 V. Nagirnyi, E. Feldbach and L. Jonsson, Energy transfer in $ZnWO_4$ and $CdWO_4$ scintillators, *Nucl. Instrum. Methods Phys. Res., Sect. ANucl. Instrum. Methods Phys. Res., Sect. A*, 2002, **486**, 395–398.

14 F. G. Yang, C. Y. Tu, J. F. Li, G. H. Jia, H. Y. Wang, Y. P. Wei, Z. Y. You, Z. J. Zhu, Y. Wang and X. A. Lu, Growth and optical property of ZnWO4:Er^{3+} crystal, *J. Lumin.J. Lumin.*, 2007, **126**(2), 623–628.

15 F. G. Yang, C. Y. Tu, H. Y. Wang, Y. P. Wei, Z. Y. You, G. H. Jia, J. F. Li, Z. J. Zhu, X. A. Lu and Y. Wang, Growth and spectroscopy of Dy^{3+} doped in $ZnWO_4$ crystal, *Opt. Mater.*, 2007, **29**(12), 1861–1865.

16 F. G. Yang, C. Y. Tu, H. Y. Wang, Y. P. Wei, Z. Y. You, G. H. Jia, J. F. Li, Z. J. Zhu, X. A. Lu and Y. Wang, Growth and spectroscopy of $ZnWO_4$:Ho^{3+} crystal, *J. Alloys Compd.*, 2008, **455**(1–2), 269–273.

17 N. Van Minh, N. Manh Hung, D. T. Xuan Thao, M. Roeffaers and J. Hofkens, Structural and optical properties of $ZnWO_4$:Er^{3+} crystals, *J. Spectrosc.J. Spectrosc*, 2013, **2013**, 424185.

18 Q. Dai, H. Song, X. Bai, G. Pan, S. Lu, T. Wang, X. Ren and H. Zhao, Photoluminescence properties of ZnWO4:Eu^{3+} nanocrystals prepared by a hydrothermal method, *J. Phys. Chem. C*, 2007, **111**(21), 7586–7592.

19 X. P. Chen, F. Xiao, S. Ye, X. Y. Huang, G. P. Dong and Q. Y. Zhang, $ZnWO_4$:Eu^{3+} nanorods: A potential tunable whitelight-emitting phosphors, *J. Alloys Compd.*, 2011, **509**(5), 1355–1359.

20 L. L. Wang, Q. L. Wang, X. Y. Xu, J. Z. Li, L. B. Gao, W. K. Kang, J. S. Shi and J. Wang, Energy transfer from Bi^{3+} to Eu^{3+} triggers exceptional long-wavelength excitation band in $ZnWO_4$:Bi^{3+}, Eu^{3+} phosphors, *J. Mater. Chem. CJ. Mater. Chem. C Mater. Opt. Electron. Devices*, 2013, **1**(48), 8033–8040.

21 X. X. Luo and W. H. Cao, Upconversion luminescence properties of Li^{+}-doped $ZnWO_4$:Yb, Er, *J. Mater. Res.*, 2008, **23**(8), 2078–2083.

22 D. Xu and J. Zang, Progress of study on upconversion laser& luminescence materials, *J. Synth. Cryst.J. Synth. Cryst*, 2001, **30**(2), 203–210.

23 Q. H. Zuo, L. H. Luo and Y. J. Yao, High Dielectric, Piezoelectric, Upconversion Photoluminescence and Low-Temperature Sensing Properties in $Ba_{0.7}Sr_{0.3}TiO_3$–$BaZr_{0.2}Ti_{0.8}O_3$:Ho/Yb Ceramics, *J. Electron. Mater.*, 2016, **45**(2), 970–975.

24 E. Kim, C. Jeon and G. Clem, "Effects of crystal structure on the microwave dielectric properties of ABO_4 (A = Ni, Mg, Zn

and B = Mo, W) ceramics", *J. Am. Ceram. Soc.*, 2012, **95**(9), 2934–2938.

25 D. Gao, X. Zhang and W. Gao, Formation of Bundle-Shaped β-$NaYF_4$ Upconversion Microtubes *via* Ostwald Ripening, *ACS Appl. Mater. Interfaces*, 2013, **5**, 9732–9739.

26 F. He, P. P. Yang, D. Wang, C. X. Li, N. Niu, S. L. Gai and M. L. Zhang, Preparation and Up-Conversion Luminescence of Hollow La_2O_3:Ln (Ln = Yb/Er, Yb/Ho) Microspheres, *Langmuir*, 2011, **27**, 5616–5623.

27 G. J. Ding, F. Cao, G. H. Wu and D. H. Bao, Bright up-conversion green photoluminescence in Ho^{3+}-Yb^{3+} co-doped $Bi_4Ti_3O_{12}$ ferroelectric thin films, *J. Appl. Phys.*, 2011, **109**, 123101.

28 G. Y. Chen, G. Somesfalean, Y. Liu, Z. G. Zhang, Q. Sun and F.P Wang, Upconversion mechanism for two-color emission in rare-earth-ion-doped ZrO_2 nanocrystals, *Phys. Rev. BPhys. Rev. B*, 2007, **75**, 195204.

29 D. He, C. F. Guo, S. Jiang, N. M. Zhang, A. C. K. Duan, M. Yin and T. Li, Optical temperature sensing properties of Yb^{3+}–Er^{3+} co-doped $NaLnTiO_4$ (Ln = Gd, Y) up-conversion phosphors, *RSC Adv.*, 2015, **5**, 1385–1390.

30 P. Haro-González, S. F. León-Luis, S. González-Pérez and I. R. Martín, Analysis of Er^{3+} and Ho^{3+} codoped fluoroindate glasses as wide range temperature sensor, *Mater. Res. Bull.*, 2011, **46**, 1051–1054.

31 P. Du, L. H. Luo and J. S. Yu, Low-temperature thermometry based on upconversion emission of Ho/Yb-codoped $Ba_{0.77}Ca_{0.23}TiO_3$ ceramics, *J. Alloys Compd.*, 2015, **632**, 73–77.

32 H. Zou, J. Li, X. S. Wang, D. F. Peng, Y. X. Li and X. Yao, Color-tunable upconversion emission and optical temperature sensing behaviour in Er-Yb-Mo codoped $Bi_7Ti_4NbO_{21}$ multifunctional ferroelectric oxide, *Opt. Mater. Express*, 2014, **4**(8), 1545–1554.

33 Q. F. Cao, X. S. Wang, Y. X. Li and X. Yao, Up-conversion luminescence and optical thermometry characterization of Ho^{3+}/Yb^{3+} co-doped $SrBi_4Ti_4O_{15}$ ferroelectric ceramics (in Chinese), *Sci Sin Tech*, 2014, **44**(12), 1254–1260.

34 X. W. Hui, Y. X. Li and X. S. Wang, Up-conversion luminescent, dielectric and ferroelectric properties of new Aurivillius oxide $Na_{0.5}Ho_{0.5-x}Yb_xBi_4Ti_4O_{15}$ (in Chinese), *Sci. Sin. Tech*, 2014, **44**(12), 1233–1237.

